JACS
JOURNAL OF THE AMERICAN CHEMICAL SOCIETY

Communication

pubs.acs.org/JACS

Plasmonic Imaging of Surface Electrochemical Reactions of Single Gold Nanowires

Yixian Wang,[†,§] Xiaonan Shan,[†,#] Hui Wang,[‡] Shaopeng Wang,[†] and Nongjian Tao*[,†,‡]

[†]Center for Bioelectronics and Biosensors, Biodesign Institute, Arizona State University, Tempe, Arizona 85287, United States
[‡]State Key Laboratory of Analytical Chemistry for Life Science, School of Chemistry and Chemical Engineering, Nanjing University, Nanjing 210093, China
[§]Department of Chemistry and Biochemistry, California State University, Los Angeles, Los Angeles, California 90032, United States
[#]Department of Electrical & Computer Engineering, University of Houston, Houston, Texas 77024, United States

Supporting Information

ABSTRACT: Nanomaterials have been widely used in energy and sensing applications because of their unique chemical and physical properties, especially their surface reactions. Measuring the local reactions of individual nanomaterials, however, has been an experimental challenge. Here we report on plasmonic imaging of surface electrochemical reactions of individual gold nanowires (AuNWs). We coated a gold thin film (plasmonic sensing layer) with a dielectric layer (Cytop) with refractive index close to that of water, and then a graphene layer for electrical contact. This design removed the interference from the sensing layer while preserving sharp surface plasmon resonance, which allowed us to obtain cyclic voltammograms of surface electrochemistry of individual AuNWs for the first time. We also investigated the difference in the electrochemical reactions of AuNWs and Au surfaces, and local distribution of electrochemical activities within a single AuNW.

Various nanomaterials have been studied and explored for chemical sensing, biomedical, and energy-related applications,[1−4] because of their unique chemical and physical properties. The traditional ensemble methods provide only averaged properties of nanomaterials with different shapes and size in a typical sample. Investigating the surface electrochemical reactions of single entities of the nanomaterials is thus essential to determine the relationship between the catalytic activities and the structure of the nanomaterials. Studying electrochemistry at the single entity level has been achieved by attaching a nanoparticle to a nanoelectrode,[5−7] collision of individual nanoparticles with a microelectrode,[8−10] or scanning probe microscopes, including scanning electrochemical microscopy,[11,12] and scanning electrochemical cell microscopy.[13] These techniques provide high sensitivity and spatial resolution but at the expense of temporal resolution and throughput. Alternatively, optical techniques, such as super-resolution fluorescence microscopy,[14−16] electrochemiluminescence,[17] dark field microscopy[18−22] have been used to study single entity electrochemistry.

Our group has recently demonstrated the capability of plasmonics-based electrochemical current microscopy (P-ECM) for studying nanomaterials directly deposited on a gold thin film (plasmonic sensing layer).[23,24] The large background signal arising from the gold film often interfere with the electrochemical reaction signals from the nanoparticles.[25,26] Here we report a P-ECM approach that can overcome the previous limitation, and demonstrate the imaging of surface electrochemical reactions of individual Au nanowires (AuNWs).

We first coated the gold film with a Cytop layer to block the background reaction of the gold film (Figure 1A). Cytop has a refractive index of 1.34, close to that of the electrolyte, so that it does not affect surface plasmon resonance (SPR). We further placed a layer of graphene on the Cytop layer, and then deposited AuNWs on the graphene layer. The graphene layer provided electrical connection to the AuNWs for potential control, yet its electrochemical reactions do not overlap with those of the AuNWs (Figure 1B). The Cytop layer is thinner than 100 nm, so that the evanescence field from the plasmonic wave reaches the AuNWs. This is shown in the plasmonic image (Figure 1C), which resolves the individual AuNWs with the distinct parabolic tails. Upon electrochemical reactions on the AuNWs, the scattering intensity changes, provide electrochemical information on each AuNW.[23] We investigated the surface electrochemistry of single AuNWs in alkaline solution, compared the surface reaction between different AuNWs, and between a single AuNW and a large Au electrode surface, and examined local redox electrochemical activity along a single AuNW.

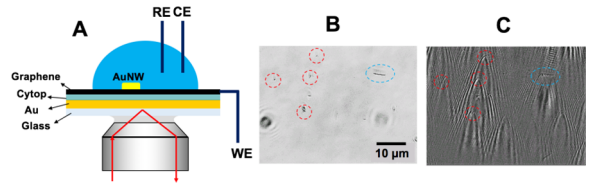

Figure 1. (A) Experimental setup. (B) Representative transmitted image and (C) SPR image of a group of 1-μm AuNWs (red circled) and a 6-μm AuNW (blue circled).

Received: October 12, 2016
Published: January 15, 2017

DOI: 10.1021/jacs.6b10693
J. Am. Chem. Soc. 2017, 139, 1376−1379

Figure 1A shows a schematic of the experimental setup. A three-electrode electrochemical cell with AuNWs (Nanopartz, 75 nm in cross-section diameter, 1 to 10 μm in length) deposited on a graphene/Cytop/Au working electrode (a Ag/AgCl as reference electrode and a Pt coil as the counter electrode) is mounted on a high numerical aperture oil immersion objective with refractive index matching oil. Light from a superluminescence diode is directed on the gold surface via the objective with a proper incident angle to excite surface plasmons, and the reflected light is collected by the same objective to form SPR images. Electrochemical reactions on the AuNWs were controlled by directly applying a potential to the graphene layer.

Representative SPR and transmitted optical images of 1-μm AuNWs (in red circles) and a 6-μm AuNW (in blue circle) are shown in Figure 1B,C. The SPR image of each nanoparticle has a parabolic tail, which is originated from the scattering of the plasmonic wave propagating along the metal film by the particle.[27] More specifically, p-polarized incident light is partially reflected (E_r) at the interface of objective/gold and partially transmitted into the gold film as an evanescent wave, which excites surface plasmons (E_{sp}). The total reflected light intensity detected in the plasmonic image is the sum of the partially reflected field and scattered plasmonic field by the object (nanowire),[28−30]

$$I_{SPR} = |E_r + \beta E_{sp}|^2 \quad (1)$$

where β describes the scattering strength that depends on the optical property (e.g., refractive index) of the nanowire.[31] Note that the first term in eq 1 produces a uniform plasmonic image, but the second term leads to a distinct parabolic pattern in the SPR image, as shown in Figure 1C. A surface electrochemical reaction at the AuNW changes the surface refractive index of the nanowire, and thus the scattering strength β, which leads to a change in the SPR image contrast of the AuNW.[32] Equation 1 can be expanded and derived to relate the change in scattering strength to the change in SPR image intensity,

$$\frac{dI_{SPR}}{dt} = 2|E_r||E_{sp}| \cos \alpha \frac{d\beta}{dt} \quad (2)$$

where α is the phase difference between the two waves. We expect that the change in β induced by a surface electrochemical reaction is proportional to the amount of the electrochemical reaction per unit time (reaction rate). Because the current density, J, is linearly dependent on the amount of electrochemical reaction per unit time, we conclude that J is related to SPR signal by

$$J = A\frac{dI_{SPR}}{dt} \quad (3)$$

where A is a constant, which was calibrated to be 2.5×10^{-4} C/m^2 by measuring the oxidation/reduction of a Au electrode in 0.2 M NaOH. Equation 3 shows that one obtains local electrochemical reaction current vs potential from the time derivative of the SPR images, or local cyclic voltammograms (CVs), from which one can study detailed reaction processes on the surface. Here we focus on imaging the local surface oxidation and reduction of single AuNWs.

Figure 2A−C show several snapshots of the P-ECM images of multiple AuNWs at different potentials, where the image contrast represents current densities (derivative of original images). The P-ECM videos of the entire oxidation and reduction processes are attached in the Supporting Information (SI) as Videos 1 and 2, respectively). At 0.06 V, which is far away from the oxidation potential of Au, there is little image contrast because no electrochemical reaction takes place (Figure 2A). As the potential increases toward the oxidation potential, contrast (current density) in the P-ECM image begins to develop (yellow) as the oxidation of Au takes place (SI video 1). The positive contrast (positive current density) reaches a maximum at 0.48 V (Figure 2B). As the potential continues to increase, the P-ECM contrast decreases and finally disappears at 0.6 V, corresponding to complete oxidation of Au atoms on the surface of the AuNWs (SI video 1). When the potential cycles back, the contrast is inverted (black), which reflects the reduction of gold oxides, and, consequently, a negative electrochemical current. The maximum negative current occurs at about −0.02 V (Figure 2C) and the P-ECM contrast disappears again when the potential cycles back to −0.2 V (SI video 2). Overlaying the optical transmission image with the P-ECM image in Figure 2D shows good correspondence between the location of the AuNWs and the vertices of the parabolic tails. Note that not all the visible AuNWs in the optical transmission image generated detectable signals in the P-ECM recordings. The absence of the electrochemical current at the AuNWs is probably due to incomplete removal of insulation layers on the surfaces of the AuNWs or graphene layer. The insets in Figure 2A−C are fast Fourier transform (FFT) in k-space, where the bright semicircles are from the scattering of the plasmonic waves by all the AuNWs in the real space P-ECM images.[33] The intensity of the semicircles increases significantly in Figures 2B,C, which further confirms that the increase in the P-ECM image contrast is from the surface reaction of AuNWs. Another interesting observation from the P-ECM video is that the maximum contrast of different AuNWs did not occur at the exactly same potential, which reveals heterogeneity in the electrochemical

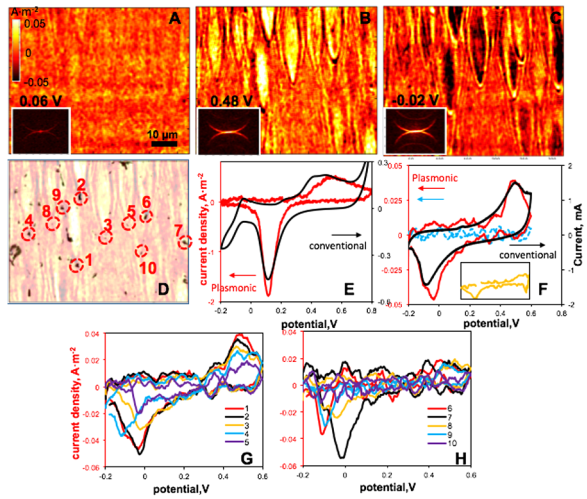

Figure 2. (A−C) P-ECM images of multiple AuNWs at different potentials. Insets are the spatial fast Fourier transfer (FFT) of the P-ECM images, which reveal a pair of semicircles. (D) Overlaying the image in panel C with the corresponding transmitted image. (E) Plasmonic (red) and conventional (black) CVs of a Au electrode. (F) Plasmonic CVs of a AuNW (red), background graphene (blue) and conventional CV (black) from the whole electrode. Inset is the CV extracted from the semicircles in the spatial FFT. (G,H) Plasmonic CVs from multiple AuNWs as labeled in panel D. The electrolyte is 0.2 M NaOH, and the potential cycling rate is 0.2 V/s.

DOI: 10.1021/jacs.6b10693
J. Am. Chem. Soc. 2017, 139, 1376−1379

activity. This level of information cannot be obtained with the ensemble measurements.

Local plasmonic CVs can be extracted from P-ECM images and compared with the conventional CVs recorded with the potentiostat. Figure 2E shows the plasmonic and conventional CVs of a Au electrode, which the plasmonic CV (red curve) is from a 1 μm × 1 μm area of the Au electrode, and the conventional CV (black curve) is from the whole electrode surface. While both the plasmonic and conventional CVs reveal major oxidation and reduction peaks around 0.5 and 0.1 V, respectively, there are differences between the two. The conventional CV reveals a large rise in the anodic current above 0.7 V, which is due to water oxidation.[34] This water oxidation does not show up in the plasmonic CV, because it does not change the optical refractive index of the surface. Likewise, the conventional CV also reveals a large cathodic current associated with oxygen reduction (<−0.1 V) that is not detected in the plasmonic CV because of the reduction product is water.[35]

The plasmonic CVs of the individual AuNWs were obtained from the P-ECM images. Figure 2F shows the plasmonic CV (red) for a single AuNW. The plasmonic CV (blue) from a graphene area adjacent to the AuNW shows no current, which confirms that the oxidation and reduction peaks are due to the AuNW. As a further control, we measured the conventional CV of the whole electrode, which shows little electrochemical reaction on the graphene surface (Figure S1A, red). As a positive control, we performed conventional CV of a layer of AuNWs deposited on a glassy carbon electrode (Figure S1B, red), and observed oxidation and reduction of the AuNWs (Figure 2F). These control experiments show that the peaks in the plasmonic CV of the single AuNW in Figure 2F is indeed due to the AuNW electrochemical reactions. Compared to the plasmonic CV of the bulk Au electrode in Figure 2E, single AuNW CV reveals a much sharper oxidation peak at ∼0.5 V, and a reduction peak at a more negative potential (∼0.0 V). Xiang et al.[36] reported a similar difference between the CVs of a bulk Au electrode and AuNWs, and attributed it to the formation of Au oxide that increases the contact resistance between the AuNWs and the supporting substrate. However, this model explains the increase separation between the oxidation and reduction peaks, but the increased sharpness in the oxidation peak of the AuNW remains an open question, and requires further studies. We measured and analyzed the plasmonic CVs of multiple AuNWs (Figure 2G,H, labeled in Figure 2D). Despite the similarities in the CVs, the shapes, positions, and amplitudes of the oxidation and reduction peaks vary among the different AuNWs. If the structures of the AuNWs are identical, then we could expect that the oxidation and reduction peak amplitudes scale with the number of surface atoms on each AuNW, which is proportional to the size of the AuNW. However, we found that peak amplitudes do not simply scale with the AuNW length linearly, and AuNWs shorter than 1 μm appear to be more active (Figure S2). This observation can be attributed to different surface structures[37] or incomplete removal of the surfactants for different AuNWs. This conclusion is consistent with the observations of large variations in the shapes and positions of the oxidation and reduction peaks of the single AuNW CVs.[36,38]

The CVs in Figure 2F−H are averaged over 19 repeated potential cycles. The complete 19 cycles from AuNW #3 are plotted in Figure S3, which shows changes in the oxidation and reduction peaks with repeated cycling of the potential. This potential cycling dependence reflects changes in the surface structure of the AuNWs associated with repeated oxidation and reduction.

P-ECM also provides local electrochemical reaction information along a AuNW. As we discussed earlier, there is a parabolic scattering tail arising from the scattering of the plasmonic wave by the AuNW along the plasmonic wave propagation direction. The spatial resolution in the perpendicular direction is limited by optical diffraction limit, which is ∼200 nm with the optics in the present experiment. We analyzed local electrochemical reaction current distribution along the AuNWs. Results from a 10 μm AuNW are shown in Figure 3, where reveal large electrochemical reaction current

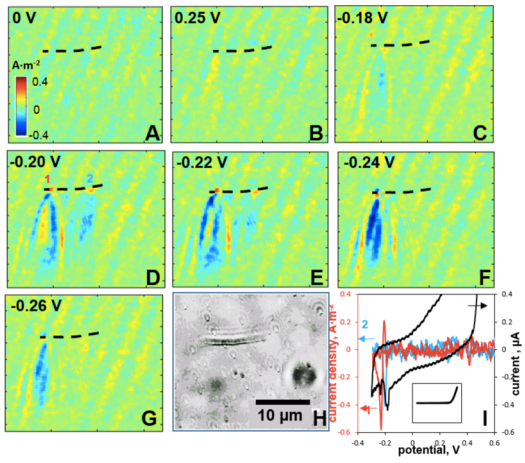

Figure 3. (A−G) P-ECM images of a 10-μm AuNW at different potentials. (H) Optical transmission image of the AuNW. (I) Plasmonic CVs from two locations on the AuNW (blue and red curves) and the conventional CV over a large ensemble of AuNWs (black curve, and see also the inset). The black dashed lines in panels A−G mark the location of the AuNW. The electrolyte is 0.2 M NaOH, and the potential cycling rate is 0.2 V/s.

near the left end of the wire. The reduction peak (maximum reduction current) occurs at ∼−0.2 V at the right end of AuNW (Figure 3D), but it occurs at a more negative potential (−0.24 V) at the left end (Figure 3F). The P-ECM images also show that the reduction peak current at the left end is much greater than that at the right end. The spatial resolution of localized detection is limited by the sensitivity of P-ECM to the surface reaction, which is about 500 nm considering the minimum surface area that can generate detectable signal.

We have demonstrated a plasmonic setup (P-ECM) for studying local electrochemical reactions at single AuNWs. By covering the Au thin film (SPR sensing surface) with a thin layer of Cytop layer and then covered with a graphene layer, we are able to remove the background current from the Au thin film surface, which allows us to image the surface oxidation and reduction of individual AuNWs, measure the CVs of the AuNWs, and compare them with those of bulk electrodes. The P-ECM images and CVs reveal differences between single AuNWs and bulk Au electrodes, large variability of different AuNWs, and location dependent reactions along a single AuNW. To fully elucidate the effects of crystal facets and microstructures on the electrochemical activities of single nanoparticles measured by P-ECM, future studies may benefit from combining P-ECM with high-resolution structural

DOI: 10.1021/jacs.6b10693
J. Am. Chem. Soc. 2017, 139, 1376−1379

imaging tools (e.g., transmission electron microscopy and scanning tunneling microscopy).

■ ASSOCIATED CONTENT

Supporting Information

The Supporting Information is available free of charge on the ACS Publications website at DOI: 10.1021/jacs.6b10693.

Experimental details and data analysis, including Figures S1−S4 (PDF)

P-ECM video 1, of the entire oxidation process (AVI)

P-ECM video 2, of the entire reduction process (AVI)

■ AUTHOR INFORMATION

Corresponding Author

*njtao@asu.edu

ORCID

Yixian Wang: 0000-0001-8691-1128

Xiaonan Shan: 0000-0001-7521-5573

Shaopeng Wang: 0000-0002-2680-0503

Notes

The authors declare no competing financial interest.

■ ACKNOWLEDGMENTS

We thank the Multidisciplinary University Research Initiative (MURI, FA9550-14-1-0003) for financial support.

■ REFERENCES

(1) Sardar, R.; Funston, A. M.; Mulvaney, P.; Murray, R. W. *Langmuir* **2009**, *25* (24), 13840−13851.

(2) Sperling, R. A.; Gil, P. R.; Zhang, F.; Zanella, M.; Parak, W. J. *Chem. Soc. Rev.* **2008**, *37* (9), 1909−1930.

(3) Saha, K.; Agasti, S. S.; Kim, C.; Li, X.; Rotello, V. M. *Chem. Rev.* **2012**, *112* (5), 2739−2779.

(4) Ishida, T.; Haruta, M. *Angew. Chem., Int. Ed.* **2007**, *46* (38), 7154−7156.

(5) Li, Y.; Cox, J. T.; Zhang, B. *J. Am. Chem. Soc.* **2010**, *132* (9), 3047−3054.

(6) Yu, Y.; Gao, Y.; Hu, K.; Blanchard, P. Y.; Noël, J. M.; Nareshkumar, T.; Phani, K. L.; Friedman, G.; Gogotsi, Y.; Mirkin, M. V. *ChemElectroChem* **2015**, *2* (1), 58−63.

(7) Clausmeyer, J.; Masa, J.; Ventosa, E.; Ohl, D.; Schuhmann, W. *Chem. Commun.* **2016**, *52*, 2408−2411.

(8) Zhou, Y.-G.; Rees, N. V.; Compton, R. G. *Angew. Chem., Int. Ed.* **2011**, *50* (18), 4219−4221.

(9) Percival, S. J.; Zhang, B. *J. Phys. Chem. C* **2016**, *120* (37), 20536−20546.

(10) Bentley, C. L.; Kang, M.; Unwin, P. R. *J. Am. Chem. Soc.* **2016**, *138* (39), 12755−12758.

(11) Sun, T.; Yu, Y.; Zacher, B. J.; Mirkin, M. V. *Angew. Chem., Int. Ed.* **2014**, *53* (51), 14120−14123.

(12) Blanchard, P.; Sun, T.; Yu, Y.; Wei, Z.; Matsui, H.; Mirkin, M. V. *Langmuir* **2016**, *32*, 2500−2508.

(13) Güell, A. G.; Meadows, K. E.; Dudin, P. V.; Ebejer, N.; Macpherson, J. V.; Unwin, P. R. *Nano Lett.* **2014**, *14* (1), 220−224.

(14) Sambur, J. B.; Chen, T.-Y.; Choudhary, E.; Chen, G.; Nissen, E. J.; Thomas, E. M.; Zou, N.; Chen, P. *Nature* **2016**, *530* (7588), 77−80.

(15) Naito, K.; Tachikawa, T.; Fujitsuka, M.; Majima, T. *J. Am. Chem. Soc.* **2009**, *131*, 934−936.

(16) Zhang, Y.; Lucas, J. M.; Song, P.; Beberwyck, B.; Fu, Q.; Xu, W.; Alivisatos, A. P. *Proc. Natl. Acad. Sci. U. S. A.* **2015**, *112* (29), 8959−8964.

(17) Wilson, A. J.; Marchuk, K.; Willets, K. A. *Nano Lett.* **2015**, *15* (9), 6110−6115.

(18) Novo, C.; Funston, A. M.; Gooding, A. K.; Mulvaney, P. *J. Am. Chem. Soc.* **2009**, *131*, 14664−14666.

(19) Hill, C. M.; Pan, S. *J. Am. Chem. Soc.* **2013**, *135*, 17250−17253.

(20) Eo, M.; Baek, J.; Song, H. D.; Lee, S.; Yi, J. *Chem. Commun.* **2013**, *49*, 5204−5206.

(21) Seo, D.; Park, G.; Song, H. *J. Am. Chem. Soc.* **2012**, *134*, 1221−1227.

(22) Byers, C. P.; Hoener, B. S.; Chang, W.-S.; Link, S.; Landes, C. F. *Nano Lett.* **2016**, *16*, 2314−2321.

(23) Shan, X.; Díez-Pérez, I.; Wang, L.; Wiktor, P.; Gu, Y.; Zhang, L.; Wang, W.; Lu, J.; Wang, S.; Gong, Q.; Li, J.; Tao, N. *Nat. Nanotechnol.* **2012**, *7* (10), 668−672.

(24) Fang, Y.; Wang, W.; Wo, X.; Luo, Y.; Yin, S.; Wang, Y.; Shan, X.; Tao, N. *J. Am. Chem. Soc.* **2014**, *136* (36), 12584−12587.

(25) Wang, Y.; Shan, X.; Cui, F.; Li, J.; Wang, S.; Tao, N. *Anal. Chem.* **2015**, *87* (1), 494−498.

(26) Chen, Z.; Shan, X.; Guan, Y.; Wang, S.; Zhu, J. J.; Tao, N. *ACS Nano* **2015**, *9* (12), 11574−11581.

(27) Yu, H.; Shan, X.; Wang, S.; Chen, H.; Tao, N. *Anal. Chem.* **2014**, *86* (18), 8992−8997.

(28) Berger, C. E. H.; Kooyman, R. P. H.; Greve, J. *Opt. Commun.* **1999**, *167*, 183−189.

(29) Lakowicz, J. R. *Anal. Biochem.* **2004**, *324* (2), 153−169.

(30) Leskova, T. A.; Maradudin, A. A.; Zierau, W. *Opt. Commun.* **2005**, *249* (1−3), 23−35.

(31) Fang, Y.; Wang, H.; Yu, H.; Liu, X.; Wang, W.; Chen, H.-Y.; Tao, N. J. *Acc. Chem. Res.* **2016**, *49* (11), 2614−2624.

(32) Demetriadou, A.; Kornyshev, A. A. *New J. Phys.* **2015**, *17* (1), 13041.

(33) Shan, X.; Díez-Pérez, I.; Wang, L.; Wiktor, P.; Gu, Y.; Zhang, L.; Wang, W.; Lu, J.; Wang, S.; Gong, Q.; Li, J.; Tao, N. *Nat. Nanotechnol.* **2012**, *7* (10), 668−672.

(34) Burke, L. D.; Nugent, P. F. *Gold Bull.* **1997**, *30* (2), 43−53.

(35) Marković, N. M.; Adić, R. R.; Vešović, V. B. *J. Electroanal. Chem. Interfacial Electrochem.* **1984**, *165* (1−2), 121−133.

(36) Xiang, C.; Güell, A. G.; Brown, M. A.; Kim, J. Y.; Hemminger, J. C.; Penner, R. M. *Nano Lett.* **2008**, *8* (9), 3017−3022.

(37) Hamelin, A.; Sottomayor, M. J.; Silva, F.; Chang, S. C.; Weaver, M. J. *J. Electroanal. Chem. Interfacial Electrochem.* **1990**, *295* (1−2), 291−300.

(38) Plowman, B. J.; Thompson, N.; O'Mullane, A. P. *Gold Bull.* **2014**, *47* (3), 177−183.

DOI: 10.1021/jacs.6b10693
J. Am. Chem. Soc. 2017, 139, 1376−1379